Surface structure of polar $Co_3O_4$(111) films grown epitaxially on Ir(100)-(1 × 1)



2008 J. Phys.: Condens. Matter 20 265011

(http://iopscience.iop.org/0953-8984/20/26/265011)

J. Phys.: Condens. Matter **20** (2008) 265011 (6pp) doi:10.1088/0953-8984/20/26/265011

# Surface structure of polar $Co_3O_4(111)$ films grown epitaxially on Ir(100)-(1 × 1)

**W Meyer, K Biedermann, M Gubo, L Hammer and K Heinz**

Lehrstuhl für Festkörperphysik, Universität Erlangen-Nürnberg, Staudtstraße 7, D-91058 Erlangen, Germany

E-mail: klaus.heinz@physik.uni-erlangen.de

Received 3 March 2008, in final form 15 May 2008
Published 28 May 2008
Online at stacks.iop.org/JPhysCM/20/265011

**Abstract**

Cobalt oxide films were prepared by oxidation of different amounts of cobalt deposited on Ir(100)-(1 × 1), where oxygen rich conditions were applied during deposition. The resulting oxide films with thicknesses of up to about 40 Å were investigated as regards their crystallographic structure and morphology, applying quantitative low energy electron diffraction (LEED) and scanning tunnelling microscopy (STM). It can be unequivocally shown that the spinel-type $Co_3O_4$ phase develops, for which an excellent fit between measured and calculated LEED intensity spectra is achieved (Pendry $R$-factor $R = 0.124$). In spite of the quadratic unit cell of the substrate the oxide films are in the polar (111) orientation. Also, the native lattice parameter of the material is assumed, i.e. there is no pseudomorphic relation to the substrate. However, by means of orientational epitaxy, one of the unit-mesh vectors of the oxide and one of those of the substrate layer are aligned, leading to two mutually orthogonal domains in the oxide. The oxide is terminated by a sublayer of cobalt ions which in the bulk were tetrahedrally coordinated $Co^{2+}$ ions. There are drastic relaxations of layer spacings at and near the surface. As a consequence, the bond length between the surface terminating cobalt ions and oxygen ions below is considerably reduced, indicative of a substantial change of the ionicity of the cobalt and/or oxygen ions. This is interpreted as accounting for polarity compensation of the film, as surface reconstruction, oxygen vacancies and species adsorbed can be ruled out.

(Some figures in this article are in colour only in the electronic version)

## 1. Introduction

The well known technical importance of the surfaces of transition metal oxides has led to intense activities in recent years in order to investigate their properties. Special interest is in oxides of magnetic metals as Fe, Co or Ni, in particular when grown as pseudomorphic thin films which allow to study the intimate relationship between structure and magnetism. The choice of Ir(100) as substrate in the present paper stems on the one hand from the fact that its lattice parameter differs substantially from those of the stable phases of cobalt oxide, so that no pseudomorphic (100) oriented oxide films can be expected. It was also motivated by our recent finding that the deposition of Fe, Co or Ni on this surface leads to the formation of nanostructures [1–3] which, according to first principle calculations, may exhibit interesting magnetic properties [4]. This makes the investigation of their oxides on the same substrate evenly interesting. In a first study of cobalt oxide on Ir(100) we retrieved that the oxidation of 1–2 monolayers thick pseudomorphic Co films leads to the formation of ultrathin films of mainly CoO [5]. In spite of the quadratic unit cell of the Ir substrate CoO appears in the polar (111) orientation with surface parallel layers in hexagonal order. Oxidation under more oxygen rich conditions produced small patches interpreted as $Co_3O_4$ in (100) orientation.

In the present work we report on thicker oxide films in the thickness range of about 20–40 Å whereby oxygen rich conditions were maintained during preparation. For the investigation of the structure and morphology of the oxide quantitative low energy electron diffraction (LEED) and scanning tunnelling microscopy (STM) were applied. In the following we first give experimental details, in particular about the preparation procedure, and then concentrate on the appearance of the films in STM and visual LEED in section 3. Subsequently, the crystallographic structure of the oxide is presented as retrieved by quantitative LEED and in the final section the results are discussed.

 

## 2. Experimental details

The experiments were performed in a two-stage ultra-high vacuum (UHV) apparatus with one of the vessels hosting a homemade four-grids LEED optics and the other a commercial beetle-type STM (RHK) with easy transfer between the two parts. Concerning the Ir(100) substrate we recall that in its stable phase it exhibits a reconstructed surface with a $(5 \times 1)$ superstructure, Ir(100)-$(5 \times 1)$-hex, in which the top layer atoms are quasi-hexagonally arranged on quadratic subsequent layers [6, 7]. The reconstruction is usually lifted by adatoms, so that a $(1 \times 1)$ phase develops. This is of almost perfect order when the reconstruction is lifted at rather elevated temperatures by adsorption of oxygen which, after the structural transition, is removed by hydrogen [8–10]. We used this well ordered and clean Ir(100)-$(1 \times 1)$ surface as support.

The cobalt oxide was prepared by deposition of Co under simultaneous $O_2$ flux and subsequent post-oxidation followed by annealing. For the metal deposition an electron-beam evaporator supplied with highly purified Co was used and operated at a deposition rate of about 1 ML min$^{-1}$ (1 ML Co corresponds to a coverage of $1.36 \times 10^{15}$ cm$^{-2}$ on Ir(100)-$(1 \times 1)$). The simultaneous oxygen flux was realized by a doser positioned in front of the sample establishing a local pressure of about $10^{-6}$ mbar. During this deposition and oxidation process a sample temperature of about 50 °C was favourable to produce rather flat films. We denote their thickness by the number of Co monolayers consumed in the oxide formation, i.e., by monolayer equivalents (MLE). Films in the thickness range of about 6–14 MLE were prepared in the way described and then, in a first step of further treatment, annealed at about 250 °C for 2 min at a local oxygen pressure of again $10^{-6}$ mbar in order to prevent any initial oxygen depletion. In a second step the films were annealed in UHV at even higher temperatures whereby, however, it was checked by thermal desorption spectroscopy that there was no significant desorption of oxygen. The respective temperatures were chosen to reach the sharpest possible LEED pattern of, as it will turn out, ideal hexagonal symmetry. They ranged from about 400 °C for 6 MLE Co to about 500 °C for 14 MLE Co. Higher annealing temperatures lead at first to a degradation of the films followed, however, by the conversion into a different long-range ordered crystallographic structure which will be addressed in a forthcoming paper. For oxides containing less than 6 MLE Co only this additional structure could be produced.

STM images could be taken only for the sample at room temperature. In contrast, LEED patterns and intensity versus energy spectra, $I(E)$, were recorded with the sample cooled by direct contact to a liquid nitrogen reservoir in order to allow for only little thermal diffuse intensities. There were no indications for surface charging. The $I(E)$ spectra were taken both for the use as fingerprints to characterize the development of the oxide as well as input for the structural analysis of the fully developed oxide. They were recorded by use of a 12-bit digital charge-coupled-device (CCD) camera viewing the LEED screen from outside the UHV, whereby the video signal is evaluated under computer control [11]. A total of 12 beams symmetrically inequivalent at normal incidence of the primary beam were measured in the range between about 50 and 600 eV in steps of 0.5 eV equivalent to an accumulated data base of energy width $\Delta E = 4664$ eV.

## 3. Appearance in STM and LEED

The appearance of the oxide films in STM and LEED depends to a certain extent on their thickness. Figure 1 displays STM images and a height histogram as well as LEED patterns and intensity spectra for films of about 6 and 14 MLE Co which were annealed at about 400 °C–500 °C, respectively. As obvious from the STM images ((a), (b)), the thicker film (b) is more homogeneous than the thinner one (a). This is consistent with the LEED patterns which show sharp spots only for the thicker film (e) in agreement with the fact that the film is dominated by islands of sizes of at least 100 Å which is in the range of the transfer width of our (conventional) LEED optics. Nevertheless, the intensity spectra for the same beam in the two films as shown in panel (k) exhibit the very same spectral features. Accordingly, the local crystallographic structure by which intensities are formed [12, 13], is identical in the two cases. Only the long-range order, which determines the spot width and profile, is poorer for the thinner oxide most probably due to the lower annealing temperature allowed in this case.

The LEED pattern displayed in figure 1(e) is shown in panels (h), (i) to consist of hexagonal patterns of two mutually orthogonal domains which, as judged by the intensity levels of the corresponding spots, are of equal weight. The hexagonal unit mesh appears in spite of the quadratic unit mesh of the substrate but, evidently, the existence of the two orthogonal domains is due to the latter. Even more, the rotational symmetry of the pattern and beam intensities is 12-fold indicative for the existence of twin domains. Evaluation of the real-space hexagonal unit-mesh length retrieves a value of 5.7 Å. Consistently, the same value results in atomically resolved STM as displayed in panel (f) of figure 1 and, in more detail, in panel (g).

A hexagonal unit mesh can be realized by both stable phases of cobalt oxide, namely the (111) orientation of CoO and of $Co_3O_4$ which own the rocksalt and normal spinel structures, respectively. In the rocksalt structure (lattice parameter $a_R = 4.260$ Å) the in-plane lattice parameter of (111) planes is $a_{R,p} = a_R/\sqrt{2} = 3.012$ Å whilst in the spinel structure ($a_S = 8.084$ Å) the value amounts to $a_{S,p} = a_S/\sqrt{2} = 5.716$ Å. Clearly, this identifies our oxide to be spinel structured in line with the oxygen rich preparation conditions. The identification of the spinel structure is also supported by the step heights of about 4.6–4.7 Å retrieved from the histogram in figure 1(c): the structural repeat length of layers in [111] direction amounts to $d_S = a_S/\sqrt{3} = 4.667$ Å (compared to 2.460 Å for the rocksalt structure). So, we take the (111) oriented spinel structure as basis for the crystallographic analysis of the oxide performed in the next section. There is obviously no correlation with the substrate's in-plane lattice parameter, $a_{Ir,p} = a_{Ir}/\sqrt{2} = 2.715$ Å ($a_{Ir} = 3.840$ Å), that is, the epitaxial growth of the oxide is non-pseudomorphic. Yet, by orientational epitaxy the $[1\bar{1}0]$

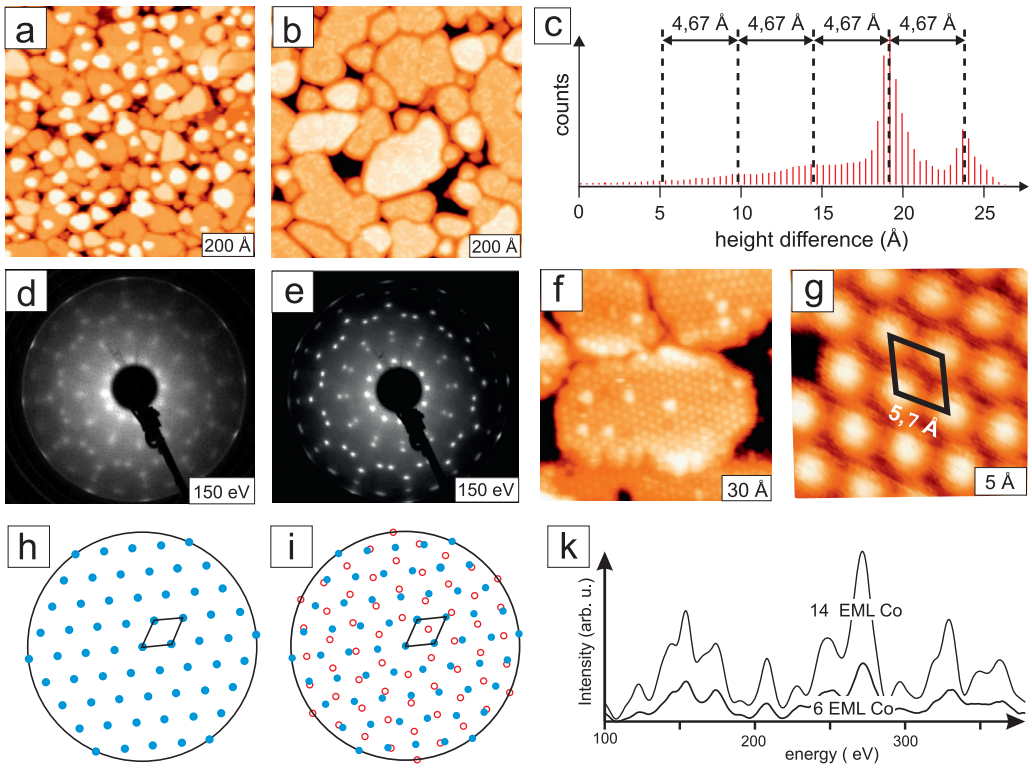


**Figure 1.** STM images and height histogram, LEED patterns and spectra for oxides with about 6 EML Co (a), (d) and 14 EML Co (b), (c), (e), (f), (g). The STM images were taken at 2.70 V (1.37 nA) for panel (a), 2.83 V (0.56 nA) for panel (b), 2.18 V (1.4 nA) for panel (f) and −2.78 V (0.67 nA) for panel (g). The STM height histogram in panel (c) is for the image in panel (b). The LEED spectra in panel (k) are for the (21) beam according to the unit mesh given in the schematic LEED patterns in panels (h), (i).

direction of the spinel film is parallel to the [011] or the $[0\bar{1}1]$ direction of the Ir substrate.

## 4. Quantitative structure determination by LEED

As obvious from the hexagonal unit mesh of the LEED pattern we can conclude that the quadratic substrate does not contribute to the measured intensities and so needs not to be considered in the intensity analysis. This is in line with the thickness of the oxide as can be calculated from the spinel structure. As displayed in figure 2 in the [111] direction there is a cobalt layer between two hexagonal oxygen layers. This either consists of a flat arrangement of $Co^{3+}$ ions in octahedral sites or is a composite layer made up by two sublayers of $Co^{2+}$ ions in tetrahedral sites and one sublayer of $Co^{3+}$ ions again in octahedral sites (one should note that due to the different coordination of $Co^{2+}$ and $Co^{3+}$ ions the oxygen layers are laterally and vertically distorted even in the bulk). In both the flat and composite layer there are three cobalt ions per hexagonal unit-mesh area, $A_{\mathrm{hex}} = a_{\mathrm{S},p}^2\sqrt{3}/2 = a_{\mathrm{S}}^2\sqrt{3}/4$. So, the thickness of the spinel oxide film results to be $D_{\mathrm{S}} = \frac{\sqrt{3}}{12}(a_{\mathrm{S},p}/a_{\mathrm{Ir},p})^2 N_{\mathrm{Co}} d_{\mathrm{S}} = (a_{\mathrm{S}}^3/12a_{\mathrm{Ir}}^2)N_{\mathrm{Co}} \approx N_{\mathrm{Co}} \times 3$ Å, whereby $N_{\mathrm{Co}}$ is the number of MLE involved. Even for $N_{\mathrm{Co}} \approx 6$ the nominal thickness of the oxide is already $D_{\mathrm{S}} \approx 18$ Å, clearly larger than the penetration length of the LEED electrons so that the substrate remains hidden to them, indeed. In the present analysis electron attenuation was simulated by an optical potential fitted to $V_{0i} = 4.5$ eV whilst the real part of the inner potential was—in view of the large energy range covered—allowed to be energy dependent according to $V_{0r} = V_{00} + V_{01}(E)$ with $V_{01}(E) = \max\{-10.25, -0.11 - 79.96/\sqrt{E/eV + 21.72}\}$ eV as calculated according to the literature [14] and with $V_{00}$ varied in the course of the analysis. Scattering phase shifts were used up to a maximum angular momentum of $l_{\max} = 13$. Following a recipe described in the literature [14, 15] they were calculated for a $Co_3O_4$ crystal with neutral atoms assumed (the issue of ionic phase shifts is addressed at the end of this section). They were corrected for thermal vibrations with the sample being at liquid nitrogen temperature for which, using the Debye-temperature $T_{\mathrm{D}} = 525$ K for $Co_3O_4$ [16], a root-mean-square (rms) vibrational amplitude of 0.067 Å results for species in the bulk. The amplitudes of oxygen and cobalt species at the surface were independently varied in the course of the structure determination. As the STM images exhibit very little defects there was no need to consider vacancies in the top layer. However, we had to consider twin domains by appropriate averaging of calculated beam intensities.

For the structural analysis we applied the perturbation method TensorLEED [11, 17, 18] using the Erlangen code [19]. As the cobalt layers are no Bravais layers they had to be treated as composite layers. The same holds for the oxygen layers due to their buckling. As indicated on the right of figure 2(a) and considering that one of the cobalt layers consists of three sublayers there are six different surface terminations possible. All of them were tested in a preliminary analysis

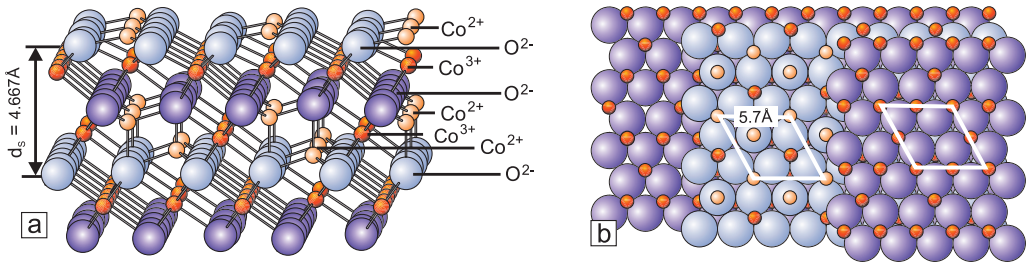


**Figure 2.** $Co_3O_4(111)$ spinel structure (a) in perspective whereby $d_S = 4.667$ Å is the vertical repeat length of layers in bulk $Co_3O_4(111)$ (disregarding the registry of layers). Panel (b) provides a top view with different layers exhibited and the hexagonal in-plane unit mesh of length $a_{S,p} = 5.716$ Å inserted in two of the layers. Large (small) balls stand for oxygen (cobalt) ions. $Co^{3+}$ ions (dark red/dark shaded) are in octahedral sites, $Co^{2+}$ ions (light red/light shaded) in tetrahedral sites.

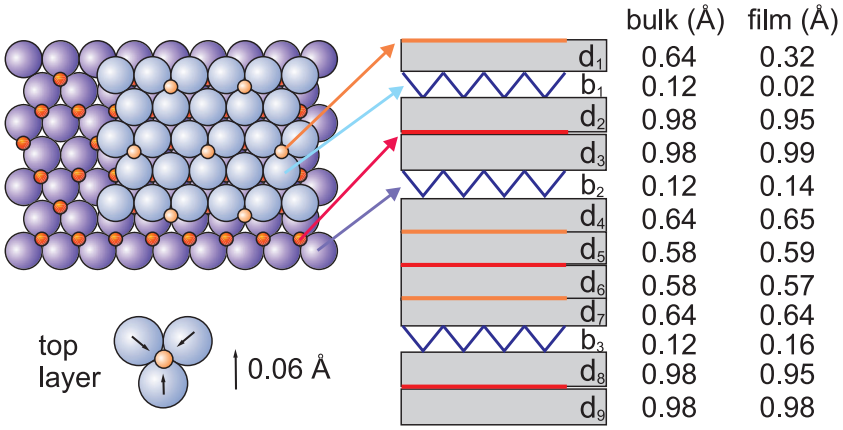


**Figure 3.** Surface structure of the $Co_3O_4(111)$ spinel-structured thin films.

using a restricted data basis with a maximum electron energy of 400 eV. Only vertical layer relaxations were allowed, that is, the spacings between the first 10 (sub)layers and the buckling of the first three oxygen layers. For the structural search a frustrated annealing procedure [20] was applied controlled by the Pendry $R$-factor [21]. This factor is also used to quantify the eventual quality of agreement between experimental and calculated best-fit model intensities.

The termination displayed in figure 2(a) produced by far the best theory-experiment fit mirrored by a Pendry $R$-factor of 0.16, whilst the values for all other terminations range between 0.31 and 0.55 so that the corresponding models can be ruled out. Refinement of the fit by allowing additionally for in-plane relaxations within the oxygen layers and including the full data base with up to 600 eV maximum energy ($\Delta E =$ 4664 eV) produced a best-fit $R$-factor as low as $R = 0.124$. A top view of this best-fit termination is displayed in figure 3 (perspective view in figure 2(a)). A sublayer of $Co^{2+}$ ions in tetrahedral coordination terminates the surface, i.e. from the total of the composite cobalt layer all $Co^{3+}$ and half of the $Co^{2+}$ ions are removed. The surface terminating cobalt and oxygen ions vibrate both with a rms amplitude of 0.10 Å and 0.12 Å, respectively. Figure 3 lists also the best-fit interlayer spacings and oxygen layer bucklings in comparison to the corresponding bulk values. There is a drastic contraction of the top layer spacing by as much as 50%. Also the buckling of the first oxygen layer is considerably reduced. The oxygen ions closest to the surface are also laterally shifted by 0.06 Å towards the $Co^{2+}$ ions to which they are coordinated (in the bulk these oxygen ions are displaced off the cobalt by 0.17 Å relative to the positions in an ideally hexagonal oxygen layer). Deeper into the surface the layer spacings are close to the bulk values. The same holds for the in-plane positions of deeper oxygen layers. The error limits as estimated by the variance of the $R$-factor [21] for the minimum $R$-factor $R$, $\mathrm{var}(R) = R\sqrt{8V_{0i}/\Delta E} = 0.011$, amount—due to the broad data basis—to only about 0.01 Å for vertical layer spacings and buckling amplitudes near the surface, increasing to about 0.02 Å when going deeper into the surface. The error limit for the in-plane relaxation in the top oxygen layer is 0.06 Å, i.e., the relaxation detected is just at the edge of the error limits.

In figure 4 experimental and best-fit spectra are compared for 6 of the 12 beams used in the analysis. Evidently, the excellent quality of the fit mirrored by the minimum $R$-factor $R = 0.124$ is also apparent from the visual comparison.

Eventually we address the issue of phase shifts entering the intensity analysis. Of course, we are aware that the scattering species are ions rather than neutral atoms for which the phase shifts used were determined. We also tried phase shifts calculated for the electronic density resulting for ionic crystal of $Co_3O_4$, again following the literature [14, 15]. Yet, the best-fit $R$-factor results as $R = 0.145$, i.e., it is beyond the $R$-factor variance worse than the agreement obtained for neutral atoms ($R = 0.124$). Accordingly, the crystallographic

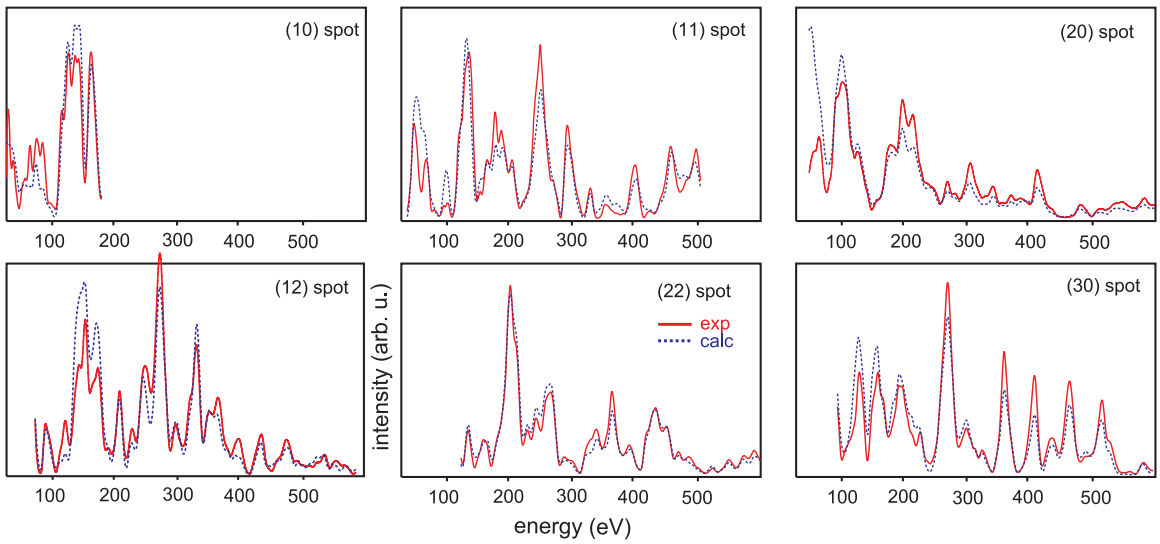


**Figure 4.** Comparison of experimental data (solid lines) and calculated best-fit spectra (dotted lines) for a selection of beams.

model parameters differ up to 0.05 Å. Using phase shifts of neutral atoms calculated for rocksalt-type CoO produces an *R*-factor as low as $R = 0.115$, whereby the model parameters differ from those given in figure 3 by only 0.01 Å at most. Again, with phase shifts calculated for ionic CoO the *R*-factor increases ($R = 0.136$) with again larger deviations of model parameters involved. As obvious for our case, phase shifts calculated for neutral atoms lead to a significantly better fit quality. This is in agreement with recent findings for $Ca_{1.5}Sr_{0.5}RuO_4(001)$ [22] but disagrees with a report for $TiO_2(110)$ [23]. On the other hand, the chemical environment for which the phase shifts were calculated (CoO or $Co_3O_4$) plays almost no role for the present system.

## 5. Discussion and conclusion

As obvious from the above results spinel-type $Co_3O_4$ develops under oxygen rich conditions on Ir(100)-(1 × 1) in the polar (111) orientation though the symmetry of the substrate is quadratic. This is the more surprising as the tetragonally coordinated $Co^{2+}$ ions form fcc sublattices with a lattice parameter of 8.084 Å which is by 'only' 5% larger than twice the value of fcc Ir, so that occupation of every second hollow site of the substrate by $Co^{2+}$ ions and further pseudomorphic oxide growth in (100) orientation from that could be imagined. Yet, the 5% contraction would be in both in-plane directions adding up to an about 10% overall closer packing. This might be energetically too unfavourable, in line with the higher surface energy for (100) compared to (111) orientation as mirrored by the fact that $Co_3O_4$ single crystals exhibit (110) and (111) crystal faces [24].

Interestingly, the same surface termination as retrieved in the present work was also found for $Fe_3O_4$ grown on Pt(111) [25]. Obviously and understandable in the light of our results, the symmetry of the substrate plays no role as well as the oxide being of inverse (rather than a normal) spinel structure with half of the 3+ ions swapped with 2+ ions, so that tetrahedral sites are occupied by $Fe^{3+}$ and octahedral ones by both, $Fe^{3+}$ and $Fe^{2+}$. So, in case of $Co_3O_4(111)$ the surface is (nominally) terminated by $Co^{2+}$ and in case of $Fe_3O_4(111)$ by $Fe^{3+}$. Yet, in both cases originally tetrahedrally coordinated ions are the terminating species and it has been argued that this comes by the fact that in this case a minimum number of bonds are broken [25]. For the system of $Fe_3O_4(111)$/Pt(111) it has also been argued by comparison with first principles calculations that the atoms resolved by STM correspond to the top layer iron ions. Though no such calculations are available for our system we are, by analogy, inclined to assume that the protrusions appearing in our STM images also correspond to the surface terminating cobalt ions. At least this would be consistent with all our findings.

The termination of the surface with only part of a layer of cobalt ions brings us to the problem of polarity of our films. As displayed in figure 5(a) the vertical repeat length of $Co_3O_4(111)$ is $d_S = 2(R_1+R_2)$. In oxygen layers the 4 oxygen ions in the hexagonal unit mesh (area $A_{hex}$) carry a charge of $4 \times (-2e) = -8e$, whilst the 3 cobalt ions in the layer with only octahedral sites carry $3 \times (+3e) = +9e$ and those in the layer with mixed sites $2 \times (+2e) + 1 \times (+3e) = +7e$. As a consequence, the total dipole moment within the repeat unit is $(7eR_2 - eR_1 + 8eR_1) = 7e(R_1 + R_2) = 7ed_S/2$ equivalent to a dipole moment density $P_S = 7ed_S/2A_{hex}$ (note that the buckling of layers plays no role in this calculation). With $N_S = \frac{\sqrt{3}}{12}(a_{S,p}/a_{Ir,p})^2 N_{Co} \approx 0.64 N_{Co}$ the number of repeat units in the film the total dipole moment density of the film below the terminating layer is $P = N_S P_S$ (figure 5(b)). With $D_S = N_S d_S$ the corresponding film thickness, a positive charge $q$ per $A_{hex}$ in the terminating layer reduces the film's polarity by $P_R = qN_S d_S/A_{hex}$, so that full compensation, that is $|P| = |P_R|$, results for $q = q_C = 7e/2$. Nominally, the charge in our terminating layer is only $q = 2e$. Additional compensation by some appropriate surface reconstruction, oxygen vacancies or ionic species adsorbed—as observed in other polar oxide films—can be ruled out in our case. This is on the basis of

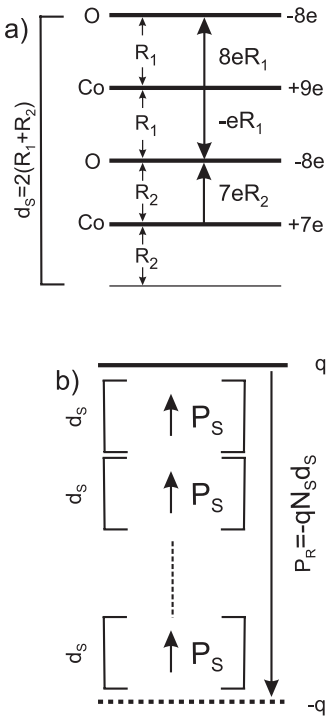


**Figure 5.** (a) Contributions to the total dipole moment of the repeat unit. Besides the layers the net charge which they carry per unit cell $A_{\mathrm{hex}}$ is given on the right and the length $d_{\mathrm{S}}$ of the repeat unit on the left. Between the layers their spacings $R_i$ are denoted (using the centre of mass planes) as well as the dipole moments caused by the charged layers. (b) Compensation model for the macroscopic dipole moment accumulated in the film.

the experimental conditions applied, the STM images and the excellent quality of our LEED fit. So, full compensation might only come by some change in the surface charge due to a corresponding change in the ionicity of the terminating cobalt or oxygen ions or, more or less equivalently, by appropriate occupation of surface states. Such a modified surface charge can easily be neutralized by charges induced in the metallic substrate near the interface.

In fact, the structure found for the film surface points towards a modified ionicity of the terminating cobalt ions. Equivalent to the substantial contraction of the top layer spacing the bond length of these ions to the oxygen ions below is reduced by 0.13 Å. This is close to the difference of radii of $Co^{2+}$ and $Co^{3+}$ (0.78 Å and 0.63 Å, respectively), so that we might have in fact a considerably increased ionicity of surface ions. $Co^{3+}$ as terminating ions would produce $q = 3e$ already rather close to $q_C$ which, formally, would correspond to $Co^{3.5+}$ ions. Alternatively, the ionicity of the top oxygen ions might be somewhat reduced. We therefore assume that a change in surface ionicity accounts for the compensation of the film's polarity.

In conclusion we have shown that, when prepared in oxygen rich conditions, cobalt oxide on Ir(100)-(1 × 1) grows as non-pseudomorphic and polar $Co_3O_4(111)$ oxide films in the range of about 20–40 Å. They exhibit the native lattice parameter of $Co_3O_4$ with the substrate only fixing the orientation of two mutually orthogonal domains via orientational epitaxy. The films are terminated by a bulk-like layer of originally tetrahedrally coordinated Co ions which had been part of a composite cobalt triple layer between two oxygen layers. Their bond length to oxygen ions below is considerably reduced indicative for a corresponding modified ionicity. This might account for compensation of the film's polarity because other mechanisms as surface reconstruction, oxygen vacancies or ionic adsorbates can be ruled out. Yet, this conclusion remains a bit speculative as, with the methods applied, we have no direct access to the surface ionicity.

## Acknowledgment

The authors are indebted to Deutsche Forschungsgemeinschaft for financial support.

## References

[1] Klein A, Schmidt A, Hammer L and Heinz K 2004 *Europhys. Lett.* **65** 830
[2] Heinz K, Hammer L, Klein A and Schmidt A 2004 *Appl. Surf. Sci.* **237** 519
[3] Heinz K, Hammer L, Klein A, Giovanardi C and Schmidt A 2004 *Acta Phys. Superfic.* **6** 43
[4] Spišák D and Hafner J 2003 *Surf. Sci.* **546** 27
[5] Giovanardi C, Hammer L and Heinz K 2006 *Phys. Rev.* B **74** 125429
[6] Ignatiev A, Jones A and Rhodin T 1972 *Surf. Sci.* **30** 573
[7] Schmidt A, Meier W, Hammer L and Heinz K 2002 *J. Phys.: Condens. Matter* **14** 12353
[8] Küppers J and Michel H 1979 *Appl. Surf. Sci.* **3** 179
[9] Heinz K, Schmidt G, Hammer L and Müller K 1985 *Phys. Rev.* B **32** 6214
[10] Lerch D, Klein A, Schmidt A, Müller S, Hammer L, Heinz K and Weinert M 2006 *Phys. Rev.* B **73** 075430
[11] Heinz K 1995 *Rep. Prog. Phys.* **58** 637
[12] Heinz K, Starke U and Bothe F 1991 *Surf. Sci.* **243** L70
[13] Heinz K 1994 *Phys. Status Solidi* a **146** 195
[14] Rundgren J 2003 *Phys. Rev.* B **68** 125405
[15] Rundgren J 2007 *Phys. Rev.* B **76** 195441
[16] Madelung O, Rössler U and Schulz M (ed) 2006 *Landolt-Börnstein* vol 41D (Berlin: Springer)
[17] Rous P J, Pendry J B, Saldin D K, Heinz K, Müller K and Bickel N 1986 *Phys. Rev. Lett.* **57** 2951
[18] Rous P J and Pendry J B 1992 *Prog. Surf. Sci.* **39** 3
[19] Blum V and Heinz K 2001 *Comput. Phys. Commun.* **134** 392
[20] Kottcke M and Heinz K 1997 *Surf. Sci.* **376** 352
[21] Pendry J B 1980 *J. Phys. C: Solid State Phys.* **13** 937
[22] Nascimento V B, Moore R G, Rundgren J, Zhang J, Cai L, Jin R, Mandrus D G and Plummer E W 2007 *Phys. Rev.* B **75** 035408
[23] Lindsay R, Wander A, Ernst A, Montanari B, Thornton G and Harrison N M 2005 *Phys. Rev. Lett.* **94** 246102
[24] Hutchison J L and Briscoe N A 1985 *Ultramicroscopy* **18** 435
[25] Ritter M and Weiss W 1999 *Surf. Sci.* **432** 81